Wind and Structures, Vol. 4, No. 5 (2001) 383-398
DOI: http://dx.doi.org/10.12989/was.2001.4.5.383

Wind induced response of an elevated steel water tank

Vincenzo Sepe† and Antonino E. Zingali‡

Dipartimento di Ingegneria Strutturale e Geotecnica, Università di Roma "La Sapienza", via Eudossiana 18, 00184 Roma, Italy

Abstract. The paper describes the results of the monitoring of an elevated steel water-tank with unusual shape, 85 m high and 40 m wide. The research was carried out analysing both the static and dynamic behaviour under wind actions. The instruments used (some of which were employed for the first time for this project) are described and the data processing procedures are discussed. Comparison between the experimental results and those obtained through a numerical model gives interesting information both on the structural behaviour and on the characterisation of wind actions.

Key words: wind effects; modal identification; monitoring; experimental tests.

1. Introduction

The paper describes the experimental investigations carried out by the Department of Structural and Geotechnical Engineering of “La Sapienza” University of Rome on an elevated water tank built on the outskirts of Rome. The steel structure, quite original from the architectonic point of view (Figs. 1 and 2) consists of a toroidal tank at about 55 m above the ground, whose cross section and mean diameter measure 4 m $\times$ 5.5 m and 30 m, respectively. Two pairs of cylindrical pillars having 3 m in diameter and a centre-to-centre distance of only 5 m support the tank.

The two pairs of pillars are diametrically opposed to each other with respect to the ring-shaped tank: one is joined to it internally while the other externally. The pillars of the first pair end at the level of the tank, and contains the dissipation basin with its pipeline and the diversion tube, respectively. The second pair of pillars contains the stairs and the lift, and reaches the maximum level of about 85 m. Beside it and joined to it there is a third tubular element, with a 7.0 m diameter which lower down decreases, by means of a truncated cone, to 3.0 m. This element acts as a piezometer and reaches the maximum height of 76.0 m. At the 70 m level there is a circular element with 15 m in diameter, including both the stairs and lift pillars and containing the collection basin which conveys the water received from the 66 m long vertical stoke pipeline into the piezometer, by means of a surge tank. In the same circular element there are a bar room and a terrace. The steel structure is partly coated with sheets of stainless steel (toroidal tank, stairs and lift pillars, piezometer, collecting basin). Foundations consists of a 3.0 m thick r.c. plate, which rests on tufaceous ground reinforced by means of jet grouting.

The structure - that is not surrounded by others high buildings - lies in the outskirts of the city, on an area that slowly declines towards the countryside in the southerly direction.

† Assistant Professor
‡ Professor

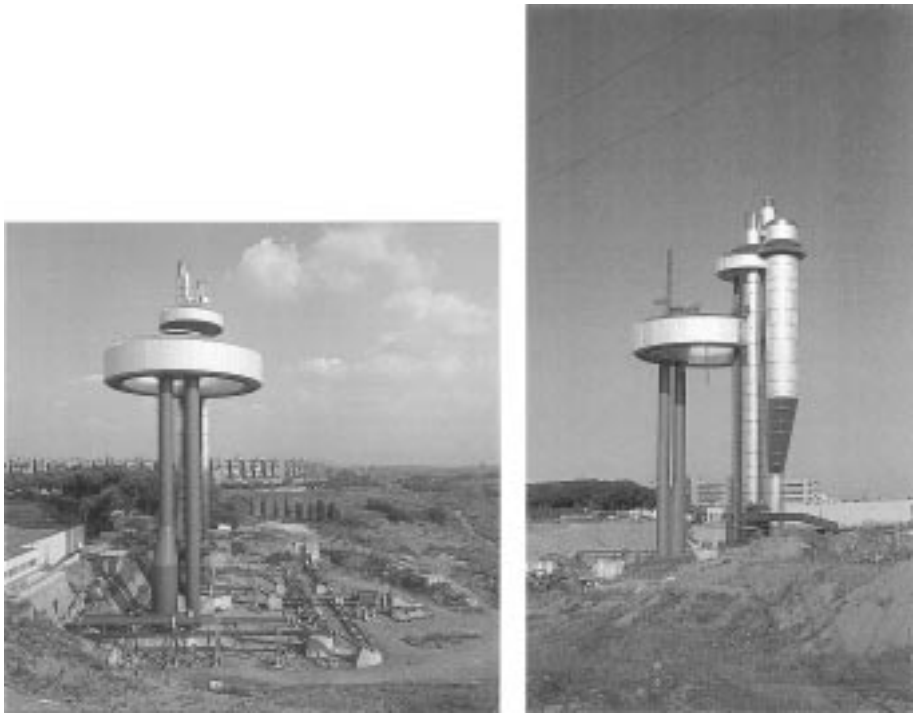

Fig. 1 West and South pictures

The symmetry axis in plan, *X*, (Fig. 2) is quite exactly oriented in *E-W* direction, so that prevailing winds, which blow along the N-S axis, impact the structure according to its lower stiffness.

Regarding the dynamic behaviour, differently from the usual slender structures (with low natural frequencies due to a rather small mass and high flexibility), in this case the sensitivity to wind is due to a large high-placed mass, and a rather large stiffness. As a consequence, there are small amplitude oscillations and low accelerations, with vibration periods of several seconds.

Other building or hydraulic details can be found in Monteverde and Romaro (1991). Preliminary results of this investigation were reported in (Zingali *et al.* 1996).

2. Numerical analysis of the structure

A preliminary structural analysis was carried out using a tridimensional model of finite linear mono-dimensional elements with about 600 d.o.f.

Due to its large stiffness, the toroidal tank behaves in the horizontal plane almost as a rigid body elastically constrained by supporting pillars, and this is evident from the first three natural modes, reported in Fig. 3, namely: *i*) cantilever-like mode, with oscillations in the *N-S* direction (*Y* axis); *ii*) shear-type mode, in the *E-W* direction (*X* axis) and *iii*) rotational mode around a vertical axis distant 11.5 m to the East from the centre of the torus, the group of pillars containing stairs, lift and piezometer being much stiffer than the other one. As shown in Table 1, the natural frequencies of the first modes are significantly influenced by the level of the water in the tank, although the modal shapes turn out to be practically unaffected; indeed the weight of the water contained in the tank

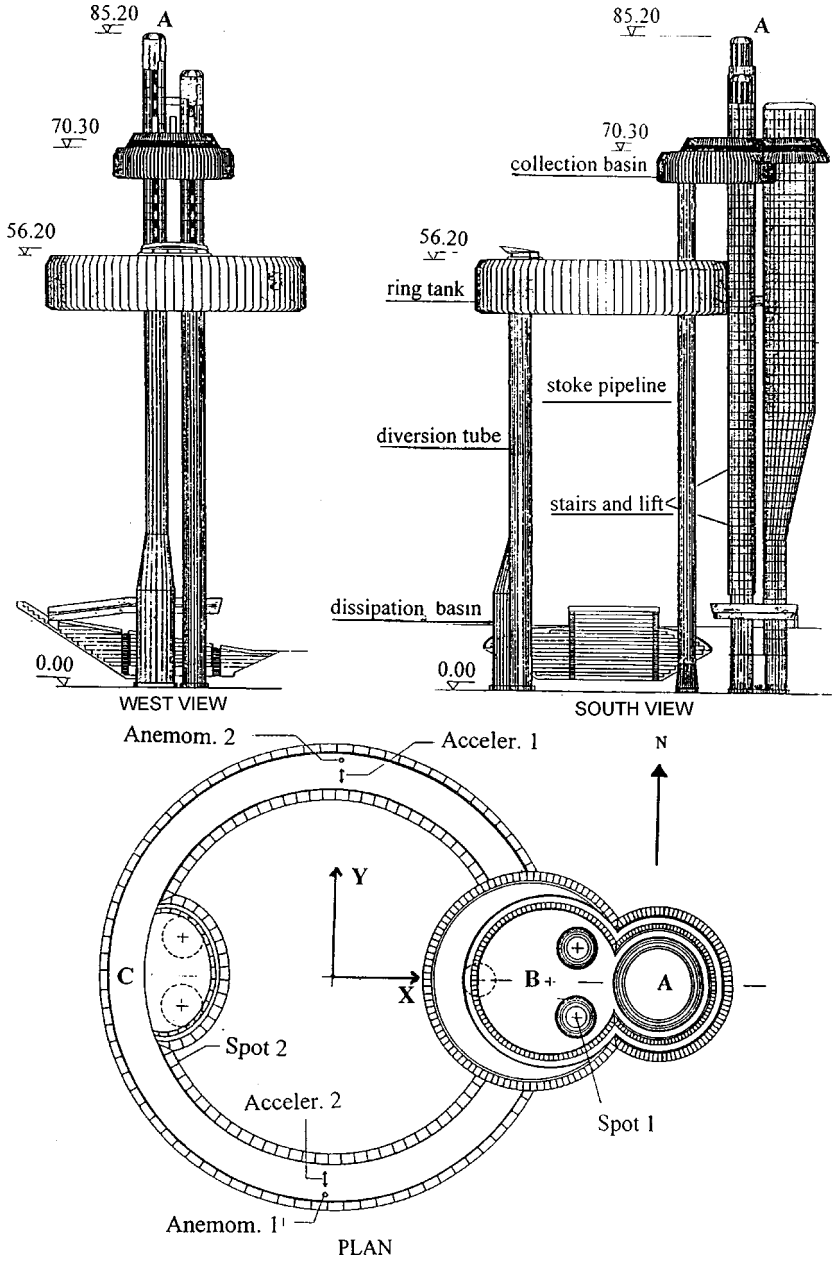

Fig. 2 West view, South view and plan

can reach 30,000 kN, which is a considerable amount if compared with the structural one of about 16,000 kN. Higher natural frequencies correspond to out-of-plane deformations of the torus or to deformations of single pillars and are not relevant on the wind-induced vibrations of the structure as a whole.

Assuming, as usual, the wind velocity as the sum of the mean value $\overline{V}(z)$ in a given time interval and of the fluctuating part $V(z, t)$, the wind induced structural response (considered as linear) can be

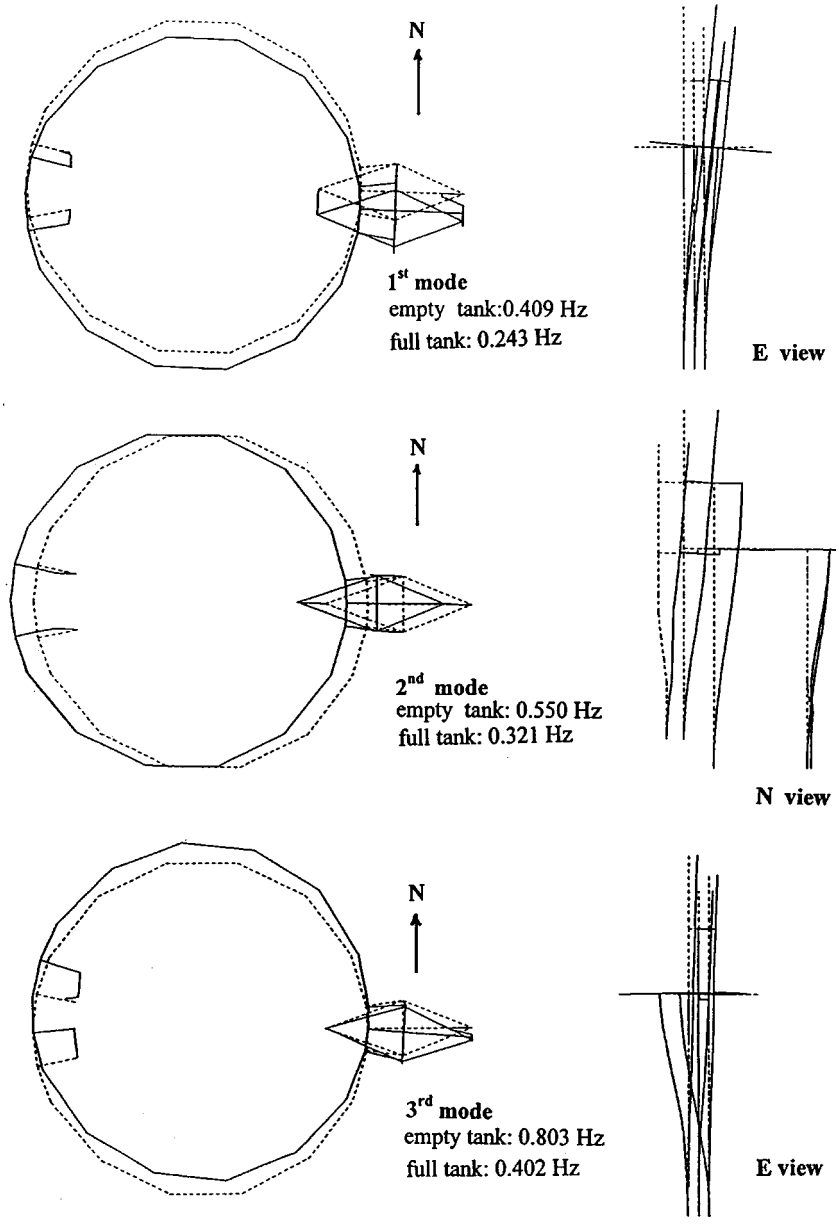

Fig. 3 Plan and view representation of the first three natural modes of the structure (diagrammatic)

Table 1 Natural periods and frequencies (calculated) of the first three natural modes

	1st mode	2nd mode	3rd mode
empty tank	2.44 s 0.409 Hz	1.82 s 0.550 Hz	1.24 s 0.803 Hz
full tank	4.10 s 0.243 Hz	3.11 s 0.321 Hz	2.49 s 0.402 Hz

divided into a static part and a dynamic one: z and t denote the level above the ground and the time, respectively.

The wind action was assumed alternately in *N-S* or *E-W* directions.

The static and dynamic analysis were carried out assuming a logarithmic vertical profile of the mean wind speed :

$$\overline{V}(z) = \frac{1}{K} u^* \ln \frac{z}{z_0}; \tag{1}$$

here z_0 denotes the roughness length, u^* is usually referred to as *shear-velocity* and the non-dimensional constant K can be assumed equal to 0.4 (Simiu and Scanlan 1996).

According to the Italian code in force at the time of the design and to the characteristics of the site, the values $z_0 = 0.3$ m and a mean wind speed $\overline{V}_{10} = 25$ m/s at 10 m level were assumed in the numerical calculations. As a consequence (cf. Eq. 1) $u^* = 2.85$ m/s and the wind speed turned out to be $\overline{V} = 39.7$ m/s at the top level of the structure ($z = 85$ m) and $\overline{V} = 37$ m/s at the level of the anemometers ($z = 56$ m); for $z \leq 8$ m a constant value $\overline{V} = \overline{V}(8\text{ m}) = 23.4$ m/s was also assumed. The logarithmic vertical profile of the mean wind speed provided in the Eurocode 1 (1995) is perfectly similar to the profile assumed, although it turns out values of the mean wind speed slightly smaller. Indeed, this difference has no relevance at all in the comparison between experimental and numerical results, that is the main objective of this paper.

The "static" along-wind force developed on a prismatic body of indefinite length, by wind orthogonal to its axis, is given, for unit length, by

$$F_D = \frac{1}{2} \rho B \overline{V}^2 C_D \tag{2}$$

where B is a typical linear dimension of the cross section of the body, and C_D is a drag coefficient depending on its shape.

According to the data available in the scientific literature (Simiu and Scanlan 1996), the following drag coefficients were used : $C_D = 0.7$ for all the bodies with circular cross section directly exposed to the wind action and $C_D = 0.4$ for those in the wake of other bodies, assuming B as the cross section diameter. For the toroidal tank (whose cross section is rectangular with blunted corners) and for the circular collection basin, $C_D = 1.9$ was assumed in the parts orthogonally acted on by the wind, B in Eq. (2) denoting now the height of the cross section. For wind with an increasing angle of incidence, C_D was correspondingly reduced until to zero for wind tangent to the body. No further reduction of C_D was introduced for the leeward half-circle of the torus, due to its large distance from the windward one (30 m along the diameter).

The static analysis on the finite elements model turned out the results in Table 2, where the point A denotes the top of the structure and B and C two points at the ends of the *E-W* diameter of the toroidal tank (see Fig. 2).

It is worth to observe that the small displacements v_s in Y direction due to wind in the X direction are due to the imperfect symmetry of the structure with respect to the X axis, caused by the dissipation basin. It can also be observed that the large surface exposed to wind action in Y direction by the group of pillars containing stairs, lift and piezometer, causes the resultant of wind forces to act on the same side of point A with respect to the rotational axis of the torus (see Sec. 2), although the axis itself is much closer to the group of pillars containing A than to the other one.

Table 2 Static analysis (numerical). Displacements components u_s and v_s in the X and Y directions (in mm). Location of points A, B, C is shown in Fig. 2, z denoting their height above the ground

	A (z = 85.1 m)		B (z = 52.18 m)		C (z = 52.18 m)	
Displacement component	u_s	v_s	u_s	v_s	u_s	v_s
Wind in X direction	53.7	1.7	36.1	1.0	36.1	0.0
Wind in Y direction	0.8	103.1	0.8	59.4	0.8	50.7

By means of a software implemented *ad hoc*, a dynamic analysis in the frequency domain was performed, taking into account the first three modes of the full tank and using the Power Spectral Density (PSD) $S_V(z, f)$ of the along-wind speed suggested by Kaimal (1972)

$$S_V(z,f) = u^{*2}\frac{200\bar{f}}{f(1+50\bar{f})^{5/3}}, \quad \text{with} \quad \bar{f} = \frac{fz}{\bar{V}(z)} \tag{3}$$

where f denotes the frequency in Hz and, for the case in question, $u^* = 2.85$ m/s, as already found. The correlation between loads induced by wind on different points of the structure at the same time was taken into account by means of "coherence functions" defined according to Simiu and Scanlan (1996).

The peak factor k, defined as the ratio between the maximum expected value of the dynamic component r of the response during the time T and its standard deviation σ_r, results (Simiu and Scanlan 1996) :

$$k = \left(\sqrt{2\ln(f^*T)} + \frac{0.5772}{\sqrt{2\ln(f^*T)}}\right), \quad \text{with} \quad f^* = \frac{\sqrt{\int_0^\infty f^2 S_r(f)\,df}}{\sigma_r} \tag{4}$$

where $S_r(f)$ indicates the PSD of the response r.

For $T = 600$s , the peak factor k was found to be almost constant and approximately equal to 3.3. The corresponding maximum dynamic displacements are shown in Table 3 together with the total ones and with the gust factor (ratio between the total maximum displacement and the "static" one).

Table 3 Dynamic analysis (numerical). Static displacement, amplitude of oscillation and maximum displacement in the X and Y direction are denoted by u_s , v_s , u_d , v_d and u_t , v_t , respectively (in mm). Location of points A, B, C is shown in Fig. 2, z denoting their height above the ground

	A (z = 85.1 m)		B (z = 52.18 m)		C (z = 52.18 m)	
Wind in X direction	u_d = 84.5		u_d = 56.4		u_d = 56.8	
	u_s = 53.7		u_s = 36.1		u_s = 36.1	
	u_t = 138.2		u_t = 92.5		u_t = 92.9	
Wind in Y direction		v_d = 171.1		v_d = 97.1		v_d = 84.4
		v_s = 103.1		v_s = 59.4		v_s = 50.7
		v_t = 274.2		v_t = 156.5		v_t = 135.1
Gust factor	2.57	2.66	2.56	2.63	2.57	2.66

3. Measurement instruments

Due to practical reasons, all the instruments were placed at the level of the toroidal tank (cf. Fig. 2); indeed, as shown in the previous section, the first three vibration modes (i.e., the most relevant ones) are perfectly identified by the displacements of the torus assumed as rigid in its own plane.

The instruments described below were used :

(a) Two cup anemometers with an end scale of 40 m/s, placed four meters above the upper edge of the torus and diametrically opposed in *N-S* direction (*Y* axis), so that one of them was undisturbed for whatever the wind direction.

(b) Two optical transducers (in the following sometimes referred to as "spots") to record the displacements. Each of them consists of a light source fixed to the structure to be monitored, framed by a telescope with 1000 mm of focal length provided with a photo-detector, which is fixed to the ground. The distance between the centroid of the light image ("spot") on the sensor and its four edges is evaluated by means of an electronic card and correspondingly the displacement components of the light source, referred to two orthogonal axes, are obtained. The scale of the displacements is previously calibrated by forcing a known displacement of the light source. The two sensors, opposed to each other along the *E-W* axis (Fig. 2, points B, C), recorded the absolute displacements of the torus and also followed the vibrations for the whole range of structural frequencies of interest.

(c) Two unidirectional accelerometers, placed in a horizontal position near the anemometers and oriented in the *N-S* direction (*Y* axis in Fig. 2). The gravity component due to the slope of the torus in the cantilever-like motion in *Y* direction resulted negligible in comparison with the horizontal components of motion-induced accelerations. The sensitivity of the accelerometers was 0.02 g / Volt, g being the gravitational acceleration, and they were able to measure accurately accelerations of the order of $g / 1000$ with a maximum frequency of 2.1 Hz, larger than the structural frequencies of interest.

All the signals were conveyed to a computer provided with an analogue-to-digital converter (EGAA card of the Electronics Inc., USA) controlled by a software able to programme frequency and length of each recording together with the time gap between two consecutive recordings. The software can also be set for the automatic recording of the data whenever a given signal, as the speed in one of the anemometers, exceeds a threshold value. A connection by modem enabled the remote control and the processing of the data, both in real time and by transferring the files on a remote computer.

4. Experimental investigation

During the monitoring of the structure, wind speeds up to approximately 25 m/s were recorded at the level of the toroidal tank. Although these speeds were smaller than the maximum expected one (Cf. Sec.2), the maximum measured displacements were of some centimetres, sufficient to carry out a satisfactory structural identification and to acquire useful information on static and dynamic structural behaviour.

Unfortunately, due to needs of the owner company, the plant was not yet fully working and the elevated tank was empty during the experimental investigation. Therefore it was not possible to monitor the fully loaded structure, which would have probably shown an increased sensitivity to the

wind actions due to the reduction of natural frequencies (Sec. 2). Nevertheless, as explained in the following, the available data allow a satisfactory comparison with the results of numerical model.

4.1. Calibration of instruments

The instruments described in Sec.3 need 14 connection lines with the analogue-to-digital converter: four for each optical transducer (two for each displacement component), two for each anemometer (speed and direction) and one for each unidirectional accelerometer.

Due to the characteristics of the electronic card, each record was about 164 seconds long, with 25 measurements per second (4096 recorded data for each channel).

While the anemometers and the accelerometers did not require a specific calibration, their characteristics being certified by the manufacturers, a rather difficult set up of optical transducers was necessary. In this case the precision is as much greater as more the image of the light source on the sensor prevails on the environment brightness. In the investigation here reported, optimum conditions (dark environment) can be guaranteed only for one sensor, placed inside the stairs cylindrical pillar (spot n.1, Fig. 2), while for the other one (spot n.2) that was not possible and a black screen was placed at the back of the light source. As the sensitivity of the spots depends both on the intensity of the light source and on its distance from the telescope, after several attempts two halogen bulbs with a narrow beam of light were used. A power of 75 Watt for the transducer inside the tubular pillar was used and of 100 W for the external one, respectively (n.1 and 2 in Fig. 2). In this way the precision of both optical transducers was fully satisfactory, allowing to measure, during the calibration and with several environmental conditions, displacements of some tenth of millimetre.

Since each optical transducer measures two displacement components on a plane orthogonal to the direction of observation, a preliminary numerical elaboration of measured data was also needed for the external spot (whose telescope was not on the vertical of the light source) in order to obtain the displacement components u, v in the horizontal plane (Fig. 2).

As explained in Sec. 3, the optical transducers, that can directly measure the horizontal displacements of the torus with respect to the ground, were preferred to the accelerometers in order to measure both dynamic and static effects. However, they do not allow to distinguish among different causes of displacements, particularly the thermal ones. Preliminary measurements, with no significant wind actions, showed thermal daily displacements as large as several centimetres, and therefore comparable or also larger than the expected wind-induced oscillations; the results of a one-day monitoring are shown in Fig. 4, each dot corresponding to one hour. The results given by optical transducers were successfully compared with displacements mechanically recorded by means of a 60 m long simple pendulum with a weight of 300 N, suspended inside one of the cylindrical pillars and equipped with a pencil tracking the movement.

The “zero” of the wind-induced displacements must therefore be evaluated for each recording and this can be quite difficult depending on the continuously variable environmental conditions. A simple and effective solution of this problem will be described in next section.

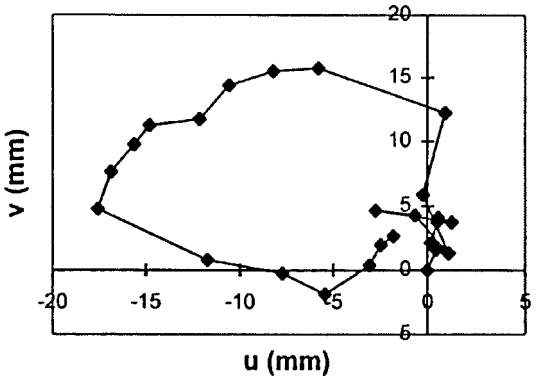

Fig. 4 *v* vs. *u* components of the one-day thermal displacement of *spot* n.1 (one dot per hour)

4.2. Static response

In order to evaluate correctly the "static" part of the structural response, corresponding to the mean wind speed, it is necessary to evaluate the displacements of the structure with respect to the configuration that it would have assumed without wind in the same environmental conditions. Therefore, for each recorded displacement time-history, the problem arises to separate the part due to wind actions from that due to different causes, assumed constant during that time-history. In the following, the technique used is described with reference to the time-history in Fig. 5, corresponding to a wind blowing almost exactly from North with a speed range of 11 to 23 m/s.

Assuming the time average on 40 seconds as sufficiently representative of the "static" response, moving averages of wind speed and displacement components on such time interval have been evaluated. Since each recording lasts approximately 160 seconds, the moving average diagrams cover a length of 120 seconds (v. Fig. 6a, b, c, e). Considering that the moving average of displacements (Fig. 6c, e) are theoretically proportional to the square of the moving average of wind speed V_m (Fig. 6b), linear regressions between displacement components u, v and V_m^2 turned out the correlation index, the slope of the regressions straight line and its intersection with the displacement axis. In most of the examined cases a very high correlation turned out, the correlation index being often higher than 0.9, especially for along-wind displacement components.

While the intersection with the displacement axis allows to obtain the "zero" of the scale, the slope p, corresponding to the ratio between the displacement and the square of the wind speed in "static" conditions, makes possible to compare the actual behaviour of the structure with the predictions of the numerical model. Namely, the experimentally identified structural stiffnesses (Cf. Sec.4.3 below) showed a very good agreement with the calculated ones, and therefore the comparison between the measured and estimated displacements is simply due to the difference between the intensity of the actual wind-induced forces and the one calculated by means of the given shape coefficients (Sec. 2). In a set of 25 successive recordings, with a wind almost exactly from North and a speed range of 10 to 25 m/s, the 20 records of displacements v along-wind with the best correlation indexes (not lower than 0.8) were considered. The mean value of the slope $p = v_m / V_m^2$ of the regression line was equal to 0.032 mm / (m/s)^2 for the point B in Fig. 2 and 0.020 mm / (m / s)^2 for the point C, with a standard deviation of about 19% and 23%, respectively.

The relatively large values of standard deviation can be explained by underlining that only wind

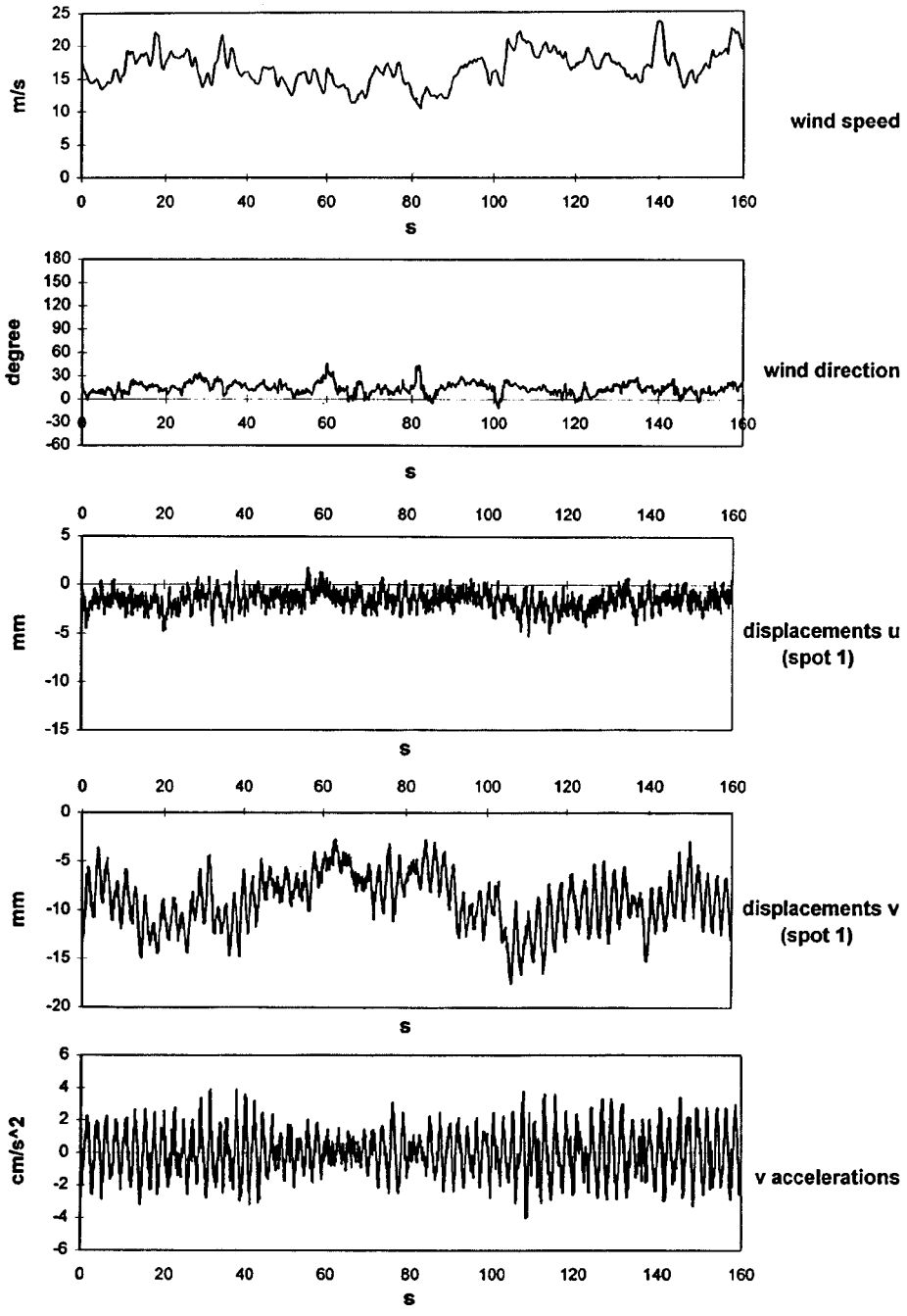

Fig. 5 A sample time-history of wind velocity, displacement components of *spot* n.1 and acceleration in the *N-S* direction

speed at a height of 56 m has been measured. Indeed the possible variations of the vertical wind profile, for a given reference speed, should be taken into account in such a structure 85 m high.

On the base of the measured data, expected displacements of the points *B* and *C* for the maximum

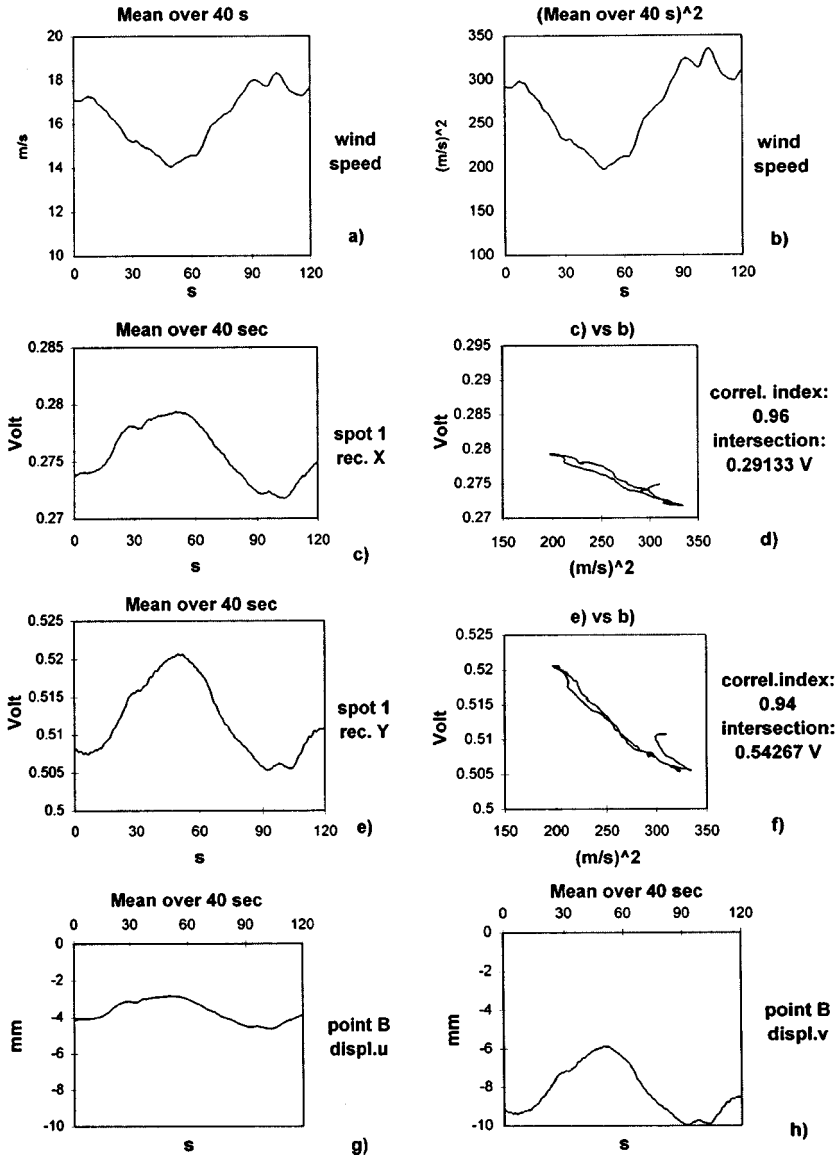

Fig. 6 Moving averages on 40 seconds for a sample time-history: a) wind speed V_m ; b) $(V_m)^2$; c-e) records corresponding to displacement components u_m , v_m of *spot* n.1 (in Volt); d-f) linear regression for u_m vs. $(V_m)^2$ and v_m vs. $(V_m)^2$; g-h) displacement components u_m , v_m (in mm) of point B in Fig. 2

design wind speed (37 m/s at the anemometers level) turn out $v_B = 43.4$ mm and $v_C = 26.7$ mm, with an error, compared to values in Table 2 (59.4 mm and 50.7 mm) of –27% and –47% , respectively.

These results suggest that the wind actions (namely, shape coefficients) introduced in the numerical model (Sec. 2) can be considered larger and therefore on the safe side with respect to the actual fluid-structure interaction. Moreover, considering that the actual rotation of the toroidal tank in the horizontal plane is larger than the calculated value, the resultant of the wind forces appears closer to the group of pillars containing stairs, lift and piezometer more than anticipated by the

numerical model.

4.3. Dynamic response

In this section the procedure of modal identification is reported; indeed, the small number of sensor locations allows to identify the first three modal shapes only. These are in perfect agreement with the results of the FEM model (Sec.2) and correspond to rigid displacements of the toroidal tank, as confirmed both by the optical transducers and by the accelerometers. The identification of higher modes would have required more sensor locations along the pillars and on the torus, so making the experimental investigation more difficult with a very small (if any) improvement of the dynamic characterisation, due to the comparatively high frequency of these higher modes. Moreover, while there has been no uncertainty on the actual shapes of the first three modes, some difference between measured and calculated modal frequencies could have been possible, due to the presence of non structural elements (e.g. as the sheets of stainless steel on some structural elements) and to the possible deformability of the foundation or of the structural joints. As shown in the following, experimental and theoretical results are instead very close to each other.

A typical wind time-history (from NNE) and the corresponding Power Spectral Density (PSD) are reported in Fig. 7a and 7b, respectively.

The PSD of the measured displacement components u_B, v_B, v_C and of the acceleration a_1 (accelerometer n.1) are reported in Fig. 7c,d,e and Fig. 7f , respectively.

Due to structural symmetry, the PSD of the displacement component u_B of the point B in the X direction (Fig. 7c) shows one significant peak only, corresponding to the second modal frequency. Similarly, the spectral analysis of the component v_B in the Y direction shows one peak only corresponding to the first modal frequency: the contribution of the third mode (torsional) on the point B displacement is in fact negligible due to the closeness to the rotation axis of the torus (Cf. Fig. 2 and Fig. 3). On the other hand, the spectral analysis of v_C and a_1 (Fig. 7e, f) shows two distinct peaks, due to the first and to the third mode.

The identification of structural properties of the first mode (frequency and damping coefficient) has been performed on the base of the PSD of v_B (Fig. 7d) that, according to numerical results (Sec.2), is the largest displacement component for wind in the NNE direction.

As it is well known (Simiu and Scanlan, 1996), when wind speed fluctuations are small compared to the mean value, the dynamic part of the wind-induced load is proportional to the fluctuating part of the wind speed. The measured time-history (Fig. 7a) being approximately stationary, the following relationship then holds between the wind speed PSD S_V(Fig. 7b) and the PSD S_F of a modal component of the wind-induced load on the structure

$$S_F(f) = C^2 S_V(f), \tag{5}$$

where for each mode the constant C depends on the geometry and on the aerodynamic characteristics of the system.

Since the modal frequencies are well separated from each other and moreover the PSD S_v of the displacement component v_B is almost exclusively due to the first mode contribution (Fig. 7d), around the first natural frequency f_1 the force - displacement relationship of a one degree-of-freedom (1 d.o.f.) linear system can be assumed, that is

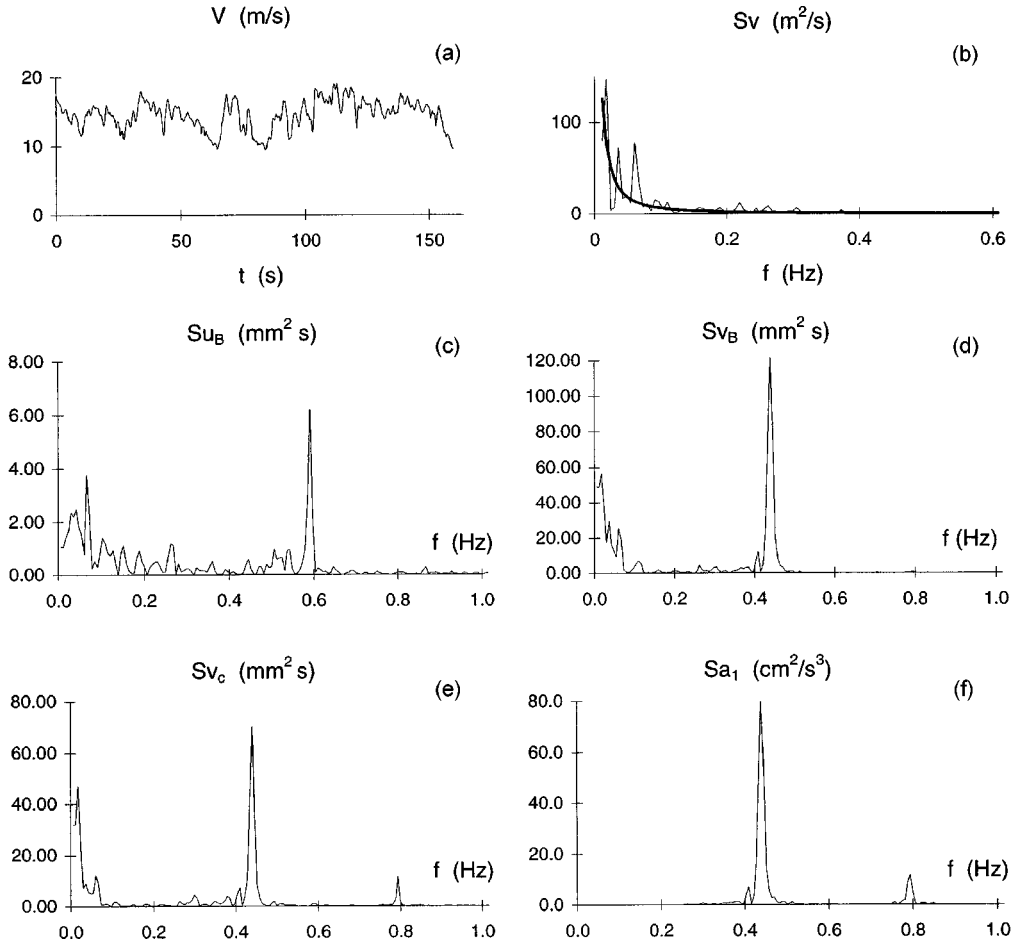

Fig. 7 (a) sample time-history of wind speed; mean value $\overline{V} = 14.5$ m/s, r.m.s. $\sigma_V = 2.09$ m/s, turbulence intensity $I = \sigma_V / \overline{V} = 0.144$; (b) power spectral density (PSD) of wind speed (thin line) and corresponding Kaimal spectrum (thick line); (c-e) PSD of displacement components u_B, v_B, v_C; (f) PSD of acceleration a_1 in *N-S* direction

$$S_v(f) = |H_1(f)|^2 S_F(f) = C^2 |H_1(f)|^2 S_V(f) \tag{6}$$

where $H_1(f)$ is the complex transfer function.

Denoting the first modal stiffness by k_1 and the first mode dynamic magnification factor (DMF) by $D_1(f) = k_1 |H_1(f)|$, it results also

$$S_v(f) = \frac{C^2}{k_1^2} D_1^2(f) S_V(f) \tag{7}$$

where for a theoretical model

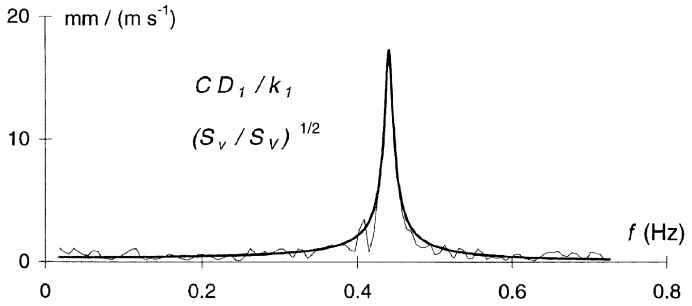

Fig. 8 Identification of the first mode characteristics for the time-history in Fig. 7. Thin line: curve $(S_v(f)/S_V(f))^{1/2}$ as measured; thick line: theoretical curve $CD_1(f)/k_1$ for a 1-d-o-f model (Eq. 7,8) with natural frequency $f_1 = 0.441$ Hz, critical damping ratio $\xi_1 = 0.011$ and $C/k_1 = 0.38$ mm/(m/s), that minimise the mean quadratic error.

Table 4 Comparison between calculated and measured natural frequencies (cf. Table 1, empty tank)

	Natural frequency (measured)	Difference with respect to analysis
1st mode	0.44 Hz	+7.6%
2nd mode	0.59 Hz	+7.3%
3rd mode	0.79 Hz	−1.6%

$$D_1(f) = \frac{1}{\left[\left(1-\left(\frac{f}{f_1}\right)^2\right)^2 + \left(2\xi_1\frac{f}{f_1}\right)^2\right]^{\frac{1}{2}}} \tag{8}$$

and C^2/k_1^2 equals the ratio S_v/S_V for $f = 0$.

An estimation of C^2/k_1^2, f_1, ξ_1 can therefore be obtained (cf. Eq. 7,8) by minimising the mean quadratic error between the theoretical curve $CD_1(f)/k_1$ and the experimental curve $(S_v(f)/S_V(f))^{1/2}$, as shown in Fig. 8. The resulting values are $f_1 = 0.441$ Hz, $\xi_1 = 0.011$ and C/k_1=0.38 mm/(m/s).

The natural frequency of the following two modes results from Fig. 7. As it is evident from Table 4, in all these cases the measured natural frequencies show a very good agreement with results of numerical analysis.

A comparison has also been performed between the measured power density spectra of wind turbulence and the theoretical predictions (Kaimal spectrum, Eq. 3). The results for two 10 minutes wind time-histories, reported in Fig. 9, show that the experimental evaluation of the spectra is in good agreement with the theoretical predictions; however, the experimental root mean square (r.m.s.) value σ_V of wind speed fluctuations and the turbulence intensity $I = \sigma_V/\overline{V}$ turn out to be smaller than the corresponding values of the Kaimal spectrum (where $\sigma_{VK} = \sqrt{6}u^*$, cf. Simiu and Scanlan, 1996); this can explain why for several time-histories, including those in Fig. 9, the experimental ratio between the maximum structural displacement and the "static" one (gust factor G) resulted smaller (mean value $\mu_G = 2.3$, standard deviation $\sigma_G = 0.1$) than the corresponding numerical values (Table 3).

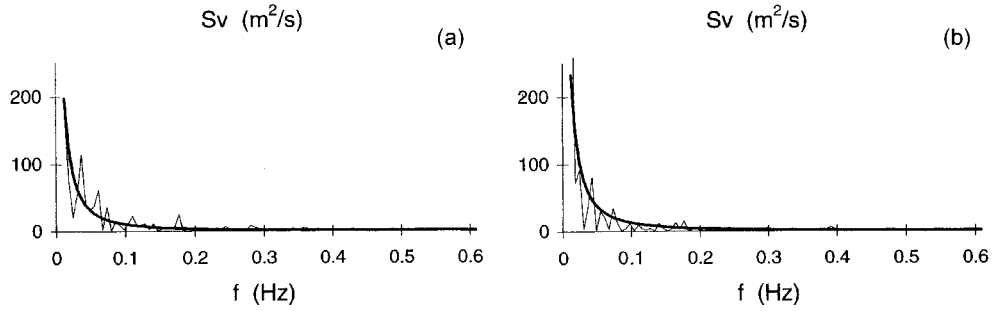

Fig. 9 Comparison between the measured power density spectrum of wind turbulence (10 minutes time-history) and the Kaimal spectrum. (a) mean wind speed $\overline{V}$ = 17.9 m/s, experimental r.m.s. of wind speed fluctuations σ_V = 2.4 m/s, turbulence intensity $I = \sigma_V / \overline{V}$ = 0.135, Kaimal r.m.s. $\sigma_{VK} = \sqrt{6}u^*$ =3.3 m/s; (b) $\overline{V}$ = 19.4 m/s, σ_V = 2.7 m/s, I = 0.14, σ_{VK} = 3.6 m/s.

5. Conclusions

The paper describes the monitoring of an elevated steel water tank under wind loading and the identification of its static and dynamic structural properties and aerodynamic characteristics.

According to what was exposed in the previous sections, the following conclusions can be drawn.

In spite of its complexity, schematising the structure by means of a tridimensional model with finite mono-dimensional linear elements resulted adequate and allowed a rather good approximation of its static and dynamic behaviour, as pointed out by the structural identification.

The PSD of the wind speed obtained by means of experimental recording is in a good agreement with those suggested by the scientific literature. The mean wind action on the structure resulted to be a little lower than those numerically evaluated by assuming values of the shape coefficients as suggested in literature. Also the observed gust factor resulted a little lower than the calculated one.

Therefore, numerical analyses turned out acceptable and safe results both for the wind action and for the structural response, with respect to the actual measured data.

As explained, the monitoring was performed with the tank empty, due to needs of the owner company. It could be useful, in the future, to repeat the monitoring with the tank full, because of the greater sensitivity of the structure to wind action expected in this case, due to the decrease of natural frequencies.

Acknowledgements

This research was coordinated by Prof. A. E. Zingali and sponsored by the Italian Ministry of University and Research, within National Research Projects on Wind Engineering (MURST 40%). Valuable discussion with Dr E. Cartapati and Dr S. Perno, both of the Department of Structural and Geotechnical Engineering of the University of Rome “La Sapienza”, as well as the technical support of the laboratory staff are gratefully acknowledged. The ACEA S.p.A., owner of the water tank, is also acknowledged for its cooperation.

References

Eurocode 1, “Basis of design and actions on structures. Part 2-4: Actions on structures - Wind actions”, ENV 1991-2-4, May 1995.

Ewins, D.J. (1985), *Modal Testing, Theory and Practice*, Research Studies Press Ltd., John Wiley, New York.

Kaimal, J.C., Wyngaard, J.C., Izumi, Y. and Coté, O.R. (1972), “Spectral characteristics of surface-layer turbulence”, *J. the Royal Meteorological Society*, **98**, 563-589.

Monteverde, C. and Romaro, G (1991), “Load bearing steel structures in the ACEA water supply centre at Vigna Murata (EUR) Rome”, *Costruzioni Metalliche* n.4, 197-208.

Simiu, E. and Scanlan, R.H. (1996). *Wind Effects on Structures*, J. Wiley & Sons, 3rd Edition.

Zingali, A.E., Cartapati, E., Perno, S. and Sepe, V. (1996), Analisi della risposta sperimentale alle azioni eoliche di una struttura alta in acciaio, *Proc. 4th Italian Conf. on Wind Engineering IN-VENTO-96*, Trieste, September, 333-346 (in Italian).

GS